Bio-Design and Manufacturing (2020) 3:30–39
https://doi.org/10.1007/s42242-020-00062-y

RESEARCH ARTICLE

Sacrificial microgel-laden bioink-enabled 3D bioprinting of mesoscale pore networks

Lei Shao[1,2] · Qing Gao[1,2] · Chaoqi Xie[1,2] · Jianzhong Fu[1,2] · Meixiang Xiang[3] · Zhenjie Liu[4] · Liulin Xiang[5] · Yong He[1,2,6]

Received: 7 January 2020 / Accepted: 22 January 2020 / Published online: 1 February 2020

Abstract

Three-dimensional (3D) bioprinting is a powerful approach that enables the fabrication of 3D tissue constructs that retain complex biological functions. However, the dense hydrogel networks that form after the gelation of bioinks often restrict the migration and proliferation of encapsulated cells. Herein, a sacrificial microgel-laden bioink strategy was designed for directly bioprinting constructs with mesoscale pore networks (MPNs) for enhancing nutrient delivery and cell growth. The sacrificial microgel-laden bioink, which contains cell/gelatin methacryloyl (GelMA) mixture and gelled gelatin microgel, is first thermo-crosslinked to fabricate temporary predesigned cell-laden constructs by extrusion bioprinting onto a cold platform. Then, the construct is permanently stabilized through photo-crosslinking of GelMA. The MPNs inside the printed constructs are formed after subsequent dissolution of the gelatin microgel. These MPNs allowed for effective oxygen/nutrient diffusion, facilitating the generation of bioactive tissues. Specifically, osteoblast and human umbilical vein endothelial cells encapsulated in the bioprinted large-scale constructs (≥ 1 cm) with MPNs showed enhanced bioactivity during culture. The 3D bioprinting strategy based on the sacrificial microgel-laden bioink provided a facile method to facilitate formation of complex tissue constructs with MPNs and set a foundation for future optimization of MPN-based tissue constructs with applications in diverse areas of tissue engineering.

Keywords Sacrificial microgel · Gelatin methacryloyl (GelMA) · 3D bioprinting · Mesoscale pore networks (MPNs) · Tissue engineering

Introduction

Three-dimensional (3D) bioprinting has recently attracted significant attention as an emerging technology that allows the fabrication of custom tissue-like biological constructs [1–9]. In general, 3D bioprinting uses precise layer-by-layer

Electronic supplementary material The online version of this article (https://doi.org/10.1007/s42242-020-00062-y) contains supplementary material, which is available to authorized users.

✉ Qing Gao
gaoqingvc@zju.edu.cn

✉ Zhenjie Liu
lawson4001@zju.edu.cn

✉ Yong He
yongqin@zju.edu.cn

[1] State Key Laboratory of Fluid Power and Mechatronic Systems, College of Mechanical Engineering, Zhejiang University, Hangzhou 310027, China

[2] Key Laboratory of 3D Printing Process and Equipment of Zhejiang Province, College of Mechanical Engineering, Zhejiang University, Hangzhou 310027, China

[3] Department of Cardiology, The Second Affiliated Hospital of Zhejiang University, School of Medicine, Hangzhou 310009, China

[4] Department of Vascular Surgery, The Second Affiliated Hospital of Zhejiang University, School of Medicine, Hangzhou 310009, China

[5] Zhejiang University Hospital, Zhejiang University, Hangzhou 310027, Zhejiang, China

[6] Key Laboratory of Materials Processing and Mold, Zhengzhou University, Zhengzhou 450002, China

deposition of bioinks (composed of cell-laden hydrogels) to generate well-designed 3D tissue constructs, such as extrusion bioprinting. An ideal bioink should possess proper mechanical and biological properties, which are essential to ensure the structural fidelity and bio-functionality of the bioprinted tissues [10–13]. Due to their intrinsic porosity and capacity for high nutrient load, hydrogels are ideal biomaterials for the preparation of bioinks. However, despite advances in hydrogel-based bioinks, the printability of bioink is still a significant hurdle that impedes biological performance [14, 15]. Indeed, developing hydrogel-based bioinks that balance the contrasting characteristics of physical printability and biological functionality is an enduring challenge for 3D bioprinting.

In order to address the requirements of tissue engineering, hydrogel-based structures require multiple scales of pores [16]: (1) macroscale pore/channel (≥ 1 mm) for nutrient transport, much like a vascular network; however, pores of this scale cannot support tissue-like structures; (2) mesoscale pore (100 μm–1 mm) for nutrient diffusion and slow degrading to allow space for new tissue formation; (3) microscale pore (1–100 μm) for structural support and nutrient absorption/retention, such as hydrogel network, as displayed schematically in Fig. 1a. However, general 3D bioprinting research has typically used bioinks that form dense hydrogel networks with low porosity in order to maintain adequate mechanical strength and structural fidelity. These dense gels often have an inadequate supply of nutrient/oxygen, limiting the migration and proliferation of encapsulated cells [17–21]. Thus, it is preferable to design bioprinted constructs with multiple scales of porous networks that enable effective nutrient/oxygen diffusion and cell structure support, facilitating the generation of functional tissues (Fig. 1b).

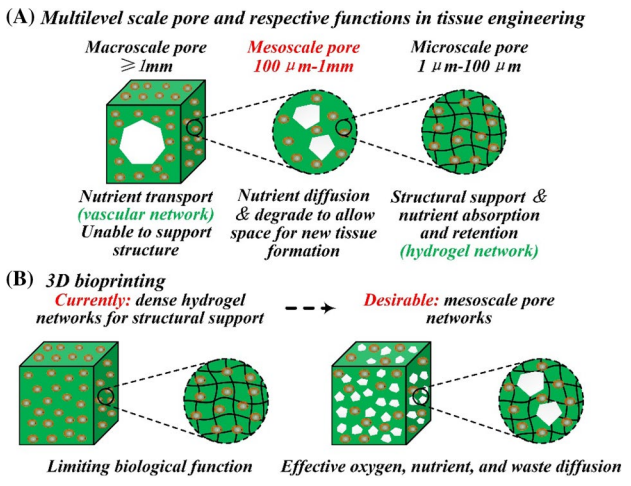

Fig. 1 **a** Multilevel scale pore and respective functions in tissue engineering. **b** Current situation and expectation of pore networks in 3D bioprinting

Porous hydrogel or void-forming hydrogel constructs have many advantages in 3D cell culture compared to non-porous tissue constructs [22]. Recently, emulsion templating has emerged as a strategy for the bioprinting of microporous hydrogel structures [23–27]. However, the micropore networks (up to several tens of micrometers) are not large enough to meet nutritional requirements of large tissue constructs. Additionally, solid particles as sacrificial templates have been used to create mesoscale porous hydrogel constructs [22]. However, 3D bioprinting hydrogel constructs with large pore sizes are challenging in practice because large solid particles tend to clog printer nozzles, especially during extrusion bioprinting. To date, there have been no methods published that describe the direct bioprinting of large-scale tissue constructs with mesoscale pore networks (MPNs).

In this work, we sought to develop a practical method for the production of a tunable and self-adapting microgel as a sacrificial template for 3D bioprinting structures with MPNs without blocking nozzle. To achieve this structure, three key components must be optimized: the choice of sacrificial ink, the microgel preparation process, and the cell-laden bioink. First, for the sacrificial ink, we believe that gelatin is an ideal choice due to its reversible thermo-crosslinking mechanism and superior biological properties. Second, to avoid blocking the print nozzle, we envisioned crushing a fully thermo-crosslinked gelatin into soft microgel prior to 3D bioprinting with the same nozzle. Finally, there are several key design characteristics for the ideal bioink, as it is the basic building block for bioprinted constructs. Importantly, the bioink should: (1) have superior biological properties to support the functionalization of cells and (2) be crosslinked during or immediately after bioprinting to maintain the structure and stabilized at physiological temperature during incubation. In recent years, gelatin methacryloyl (GelMA) has attracted increasing attention due to its excellent physicochemical and biological properties [28–39]. GelMA is a gelatin derivative, which has both reversible thermo-crosslinking mechanism and irreversible photo-crosslinking mechanism. These unique properties make gelatin and GelMA ideal bioink combination for the development of bioprinted tissue constructs with MPNs.

Herein, we developed a direct 3D bioprinting strategy capable of generating complex freeform 3D constructs with MPNs by using tunable sacrificial microgel (gelatin microgel) bioink. This strategy used reversible thermo-crosslinking mechanism (gelatin and GelMA) and irreversible photo-crosslinking mechanism (GelMA) to create a structure containing our desired design characteristics, as displayed schematically in Fig. 2a, b. We also assess the printability of the sacrificial microgel-laden bioink

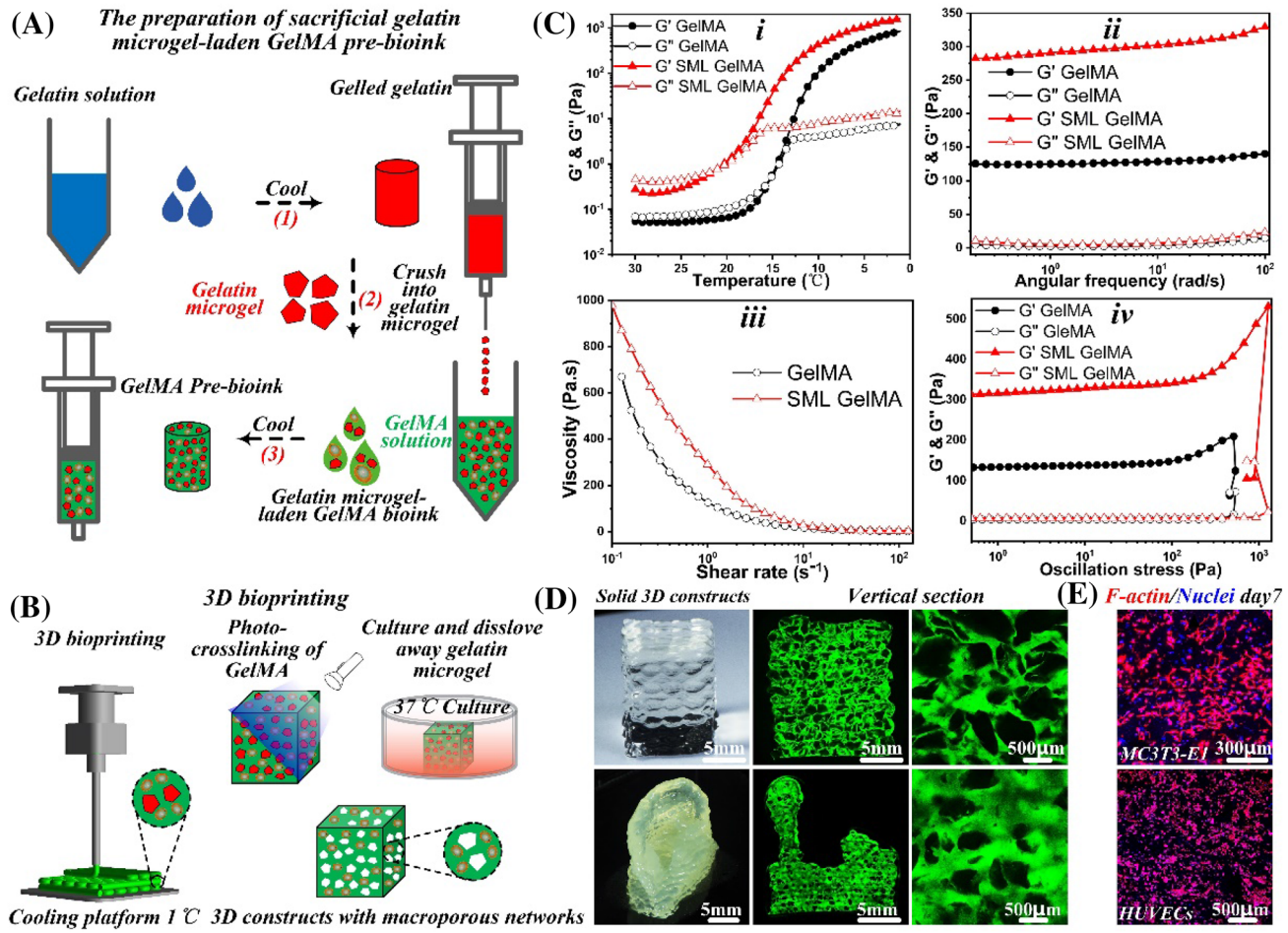

Fig. 2 3D bioprinting large-scale tissue constructs with MPNs. **a** Schematic illustration of the preparation of sacrificial gelatin microgel-laden GelMA pre-bioink. **b** The process of 3D bioprinting constructs with MPNs. **c** Characterization of the GelMA pre-bioink and sacrificial microgel-laden GelMA (SML GelMA) pre-bioink; **i** G' and G'' values as functions of temperature; **ii** mechanical spectra of the pre-bioinks at 22 °C; **iii** viscosity as a function of shear rate (22 °C); **iv** yield stress of the pre-bioinks at 22 °C. **d** Digital images of the bioprinted structure with fluorescent polystyrene nanoparticles and confocal laser scanning microscopy (CLSM) images of vertical section views showing the MPNs. **e** CLSM images showing the spreading of MC3T3-E1 cells and HUVECs encapsulated in bioprinted constructs with MPNs

through rheological experiments (Fig. 2c). Due to the cell-laden bioink and sacrificial microgel work together to promote their printability, the freeform large-scale constructs with MPNs can easily be bioprinted [Fig. 2d and Figure S1 (Supporting Information)]. Importantly, we found that osteoblasts and human umbilical cord vein endothelial cells (HUVECs) encapsulated in the bioprinted constructs could stretch, migrate, and connect during a period of culture (Fig. 2e). In light of these results, we believe that this 3D bioprinting strategy may lead to new innovations that require printing large-scale tissue constructs retaining biological function for further biomedical research or organ repair.

Results and discussion

Preparation of sacrificial gelatin microgel-laden GelMA pre-bioink

Our strategy involves the preparation of a sacrificial gelatin microgel-laden GelMA pre-bioink for direct bioprinting into temporally stable structures using reversible thermo-crosslinking mechanism (gelatin and GelMA) and subsequent irreversible photo-crosslinking of the GelMA, creating long-term stability. Similar to gelatin, the GelMA solution is liquid at 37 °C or above. However, at room

temperature (22 °C) or below, viscosity of GelMA gradually increases and reversible gelation occurs. Additionally, the GelMA can be permanently photo-crosslinked to maintain the final structure. Accordingly, sacrificial gelatin microgel-laden GelMA pre-bioink enabling extrusion bioprinting can be achieved through a simple cooling process. As displayed schematically in Fig. 2a, the sacrificial gelatin microgel-laden GelMA pre-bioink was prepared through a three-step procedure: (1) The gelatin solution was cooled down into fully gelled gelatin at − 20 °C for about 15 min in the syringe; (2) the gelled gelatin was crushed into microgel steadily and uniformly and squeezed directly into the GelMA solution through syringe needles; and (3) the sacrificial gelatin microgel-laden GelMA solution was loaded into a 10-ml syringe and mixed evenly with pipette and then cooled down into GelMA pre-bioink at − 20 °C for about 5 min for 3D bioprinting. It should be noted that during the cooling process for preparing cell-laden GelMA pre-bioink, the syringes should be flipped every 20 s to ensure that the cells and microgels were evenly dispersed in pre-bioinks. Additionally, sacrificial microgels were obtained by smooth and uniform crushing of homogeneous gelled gelatin blocks through syringe needles. Their sizes are relatively uniform, and only their shapes are irregular. Sacrificial microgels with different sizes can be prepared through syringe needles with different sizes. Furthermore, the sacrificial microgels with similar sizes can be reproduced through the same syringe needle/syringe and the same extrusion speed. Because the pore sizes were determined by the sacrificial microgel sizes, the pore sizes are relatively uniform and only their shapes are irregular.

Printability of sacrificial gelatin microgel-laden GelMA pre-bioink

To confirm that the pre-bioink could meet the requirements of extrusion-based 3D printing, the rheological properties of pure GelMA pre-bioink and SML GelMA pre-bioink were measured (Fig. 2c). Rheological properties of the bioinks were measured by a rheometer (DHR-2, TA Instruments, New Castle, DE, USA) equipped with a 40-mm parallel plate. The temperature dependence of storage modulus (G') and loss modulus (G'') was obtained using temperature sweep (oscillation) by decreasing temperature from 30 to 1 °C at a cooling rate of 5 °C/min (the frequency and shear strain were maintained constant at 10 rad/s and 5%, respectively) (Fig. 2i). When the temperature was gradually decreased to the gelation temperature about 15–22 °C, both G'' and G'' of GelMA/SML GelMA solution increased rapidly due to the formation of physical crosslinked pre-bioink. When G' was higher than G'', the pre-bioinks exhibited a gelled structure, facilitating the excellent shape fidelity of the printed structures. And the gelation temperature of SML GelMA is higher than that of pure GelMA, indicating that SML GelMA is more temperature sensitive and has better printability. The mechanical spectra were obtained at a constant strain of 5% in a frequency range of 0.1–100 rad/s at 22 °C and measured immediately after two sequential processes of cooling (4 °C, 5 min) and recovery (22 °C, 5 min) (Fig. 2ii). The GelMA and SML GelMA pre-bioink showed stable modulus, demonstrating the stability of these pre-bioinks. And the modulus of SML GelMA is higher than that of pure GelMA, indicating that SML GelMA is more robust and can better maintain the fidelity of the bioprinted structure. We further confirmed that these pre-bioinks exhibited shear thinning properties. The viscosity measurements as a function of shear rate (0–100/s) were conducted at 22 °C immediately after two sequential processes of cooling (4 °C, 5 min) and recovery (22 °C, 5 min). The viscosities of the pre-bioinks decreased with increasing the shear rates (Fig. 2iii). Thus, the pre-bioinks could be smoothly extruded from the nozzle due to the shear thinning property, and it formed stable hydrogel filaments due to the high viscosity when the shear stress was released. Moreover, the yield stress of physical crosslinked hydrogels was obtained using stress sweep (oscillation) method at a constant angular frequency of 10 rad/s under 22 °C and measured immediately after two sequential processes of cooling (4 °C, 5 min) and recovery (22 °C, 5 min) (Fig. 2iv). The yield stress of SML GelMA is higher than that of pure GelMA, also indicating that SML GelMA has better printability.

Process of bioprinting constructs with mesoscale pore networks

As displayed schematically in Fig. 2b, to fabricate 3D constructs with MPNs, the 3D bioprinting strategy was designed and had three major steps: (1) the preparation of the sacrificial gelatin microgel-laden GelMA pre-bioink; (2) 3D bioprinting temporary structure via a cooling process; and (3) permanent photo-crosslinking of GelMA and dissolving away gelatin microgel to create the final structure with MPNs. First, because the gelled gelatin microgel would melt a little bit and get a little smaller when they were added to GelMA solution, the extrusion-based 3D bioprinting could be performed using the same or larger nozzle than that was used to make the gelatin microgel. The GelMA filament-containing gelatin microgel was deposited layer by layer on the cooling platform (1 °C). It is worth noting that the whole 3D bioprinting process was performed at room temperature (22 °C) to keep the bioink printable. Then, to get permanent structures, the temporary gelled GelMA constructs were photo-crosslinked through a blue light source (405 nm, 100 mw/cm^2) for about 20 s. Last, the permanent constructs were placed on a shaker (70 rpm) for dynamic culture for 3 h in

a 37 °C incubator. During this 3 h, the reversible thermo-crosslinked gelatin microgel liquified and dissolved away to create MPNs. Subsequently, long-term dynamic culture was performed after refreshing the culture medium on the shaker (70 rpm). The strategy of pre-bioinks made it possible to print low-concentration bioinks directly, create higher porosity, and decrease stiffness. Together, we believe that this 3D bioprinting strategy is a versatile platform for engineering tissue constructs with MPNs for diverse applications in tissue engineering.

Bioprinting parameters and properties

Different pore sizes within the bioprinted constructs could be created by adjusting the extrusion nozzles used for making the gelatin microgel and 3D bioprinting. Similarly, different porosities could be achieved by adjusting the ratio of the volume of gelatin microgel to GelMA solution (Fig. 3a). By combining different extrusion nozzles (ranging from 18 to 20 G) or combining different volumes of gelatin microgel (0.5–2 ml) with a fixed volume of GelMA (2 ml), a series of constructs (10 mm × 10 mm × 10 mm) were printed. From the actual sizes (width and height) of the bioprinted samples [Figure S2 (Supporting Information)], it can be seen that the width has a good fidelity; however, due to the inevitable accumulated error on the height, the height has general fidelity. Meanwhile, by observing the vertical section, the pore sizes and porosity were analyzed. When the extrusion nozzle and the volume of GelMA solution (2 ml) were fixed, the porosity increased with the increasing volume of gelatin microgel. When the volumes of gelatin microgel and GelMA solution were fixed, the pore sizes increased with the increasing sizes of extrusion nozzles (ranging from 20 to 18 G). Next, the compression tests were performed to test the mechanical properties of the constructs (10 mm × 10 mm × 10 mm) with MPNs at room temperature, as shown in Fig. 3b. Compressive stress–strain curves of the constructs with MPNs are shown in Fig. 3c. Mechanical

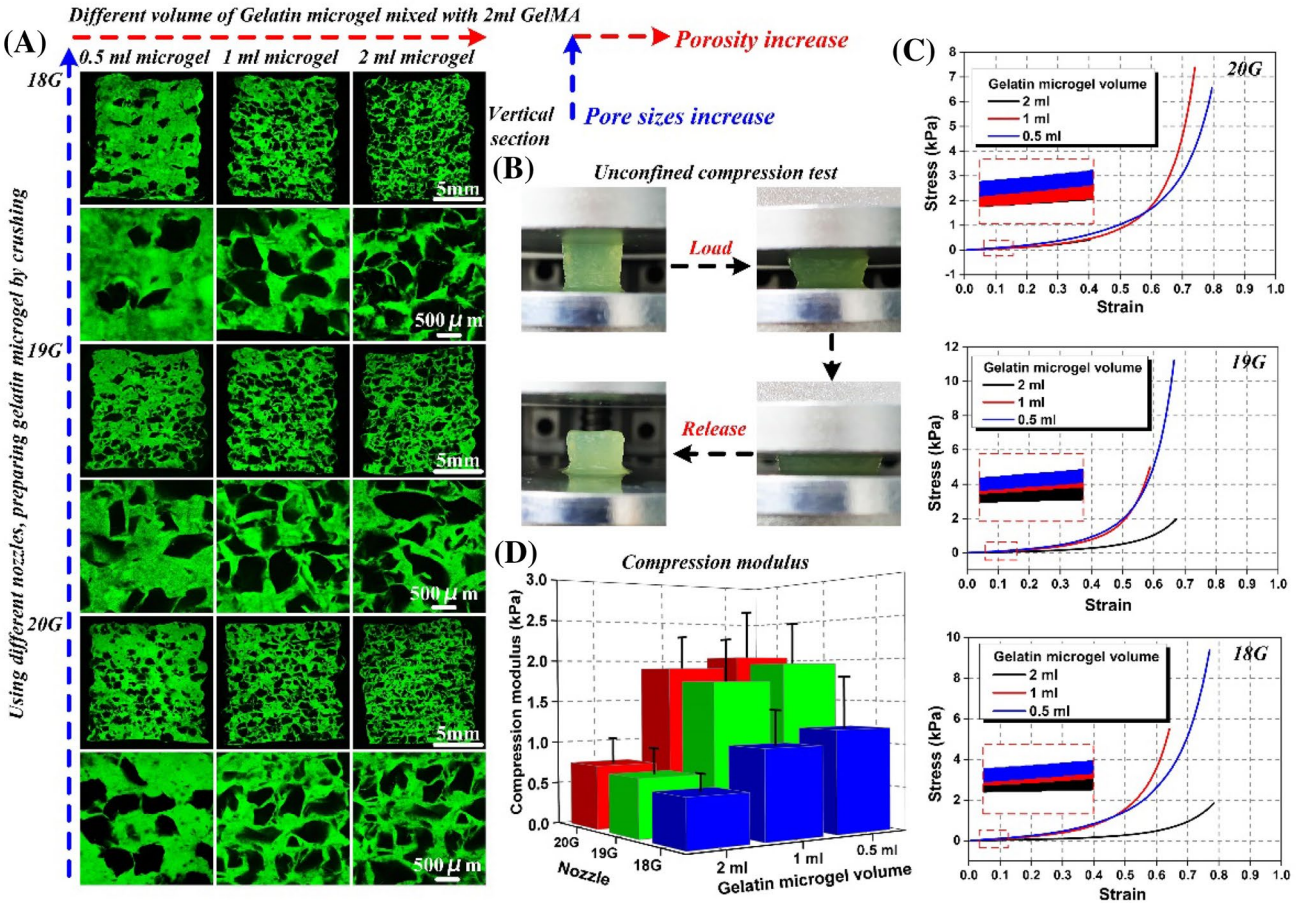

Fig. 3 Effect of varying gelatin microgel volume on porosity/pore size and mechanical properties of bioprinted constructs with MPNs. **a** CLSM images showing the change of porosity/pore sizes with changing the volume of gelatin microgel with a fixed volume of GelMA solution (2 ml) and different extrusion nozzles (18G, 19G, 20G). **b** The unconfined compression tests of the bioprinted constructs with MPNs. **c** Compressive stress–strain curves of the constructs with MPNs. **d** Compressive modulus of the bioprinted constructs with MPNs (mean values are presented and the error bars show the SD of independent replicates)

properties were characterized through compressive modulus as displayed in Fig. 3d. It was found that the compressive modulus is about 0.7–2 kPa and increases with the decrease in pore sizes and porosity. Accordingly, due to tunable pore sizes/porosity, tunable mechanical properties of the constructs with MPNs enable to meet the soft tissue needs in the relevant applications [40].

Bioprinting of complex constructs with mesoscale pore networks

To mimic the complex structural characteristics of organisms, freeform constructs with MPNs are desirable. Through 3D bioprinter, the sacrificial gelatin microgel-laden GelMA pre-bioink could be extruded and smoothly deposited to create complex constructs with desired structure, as shown in Fig. 4. We created various freeform shapes to demonstrate versatility of this bioprinting strategy. All printed structures closely resembled the morphology of the target model. Specifically, two-dimensional (2D) patterns could be printed with great fidelity (Fig. 4a). Furthermore, we found that this technique was capable of bioprinting complex organ-scale structures with MPNs, such as the nose and bone [Fig. 4b, c and Figure S3A (Supporting Information)]. More importantly, these whole bioprinted structures maintained MPNs, as seen in the vertical/cross-sectional views of different locations.

Bioprinting of heterogeneous constructs with mesoscale pore networks

To mimic the multiple cell types and the extracellular matrix (ECM) of native tissues, heterogeneous constructs with tunable compositions are highly desirable. To generate multicomponent and multicellular constructs, we designed a practical all-in-one nozzle which allowed the rapid bioprinting of constructs using different materials, as displayed schematically in Fig. 5a. Using two-in-one nozzles and varying the type of GelMA pre-bioink with gelatin microgel that was extruded separately, we bioprinted heterogeneous structures with MPNs [Fig. 5b, c and Figure S3B (Supporting Information)]. The resulting 2D patterns and 3D heterogeneous structures suggest that these all-in-one nozzles can rapidly switch between different bioinks in a fully programmable

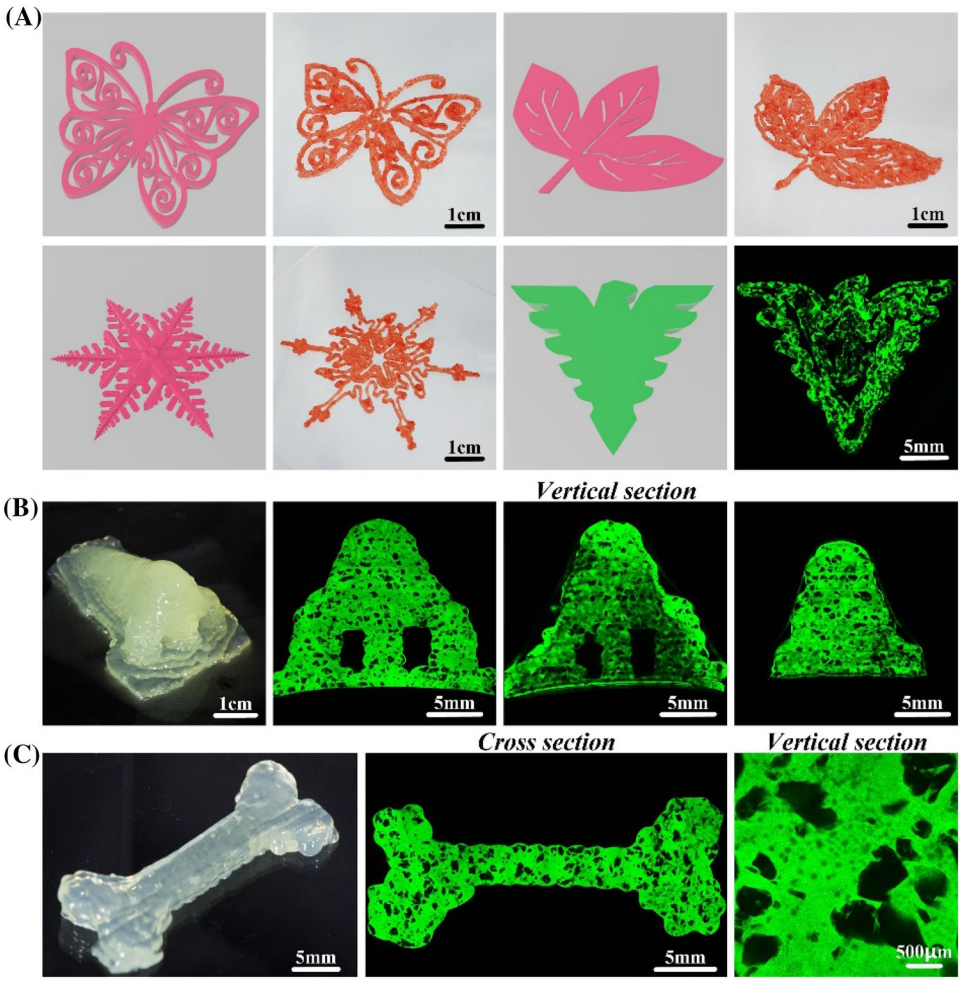

Fig. 4 Bioprinting of complex constructs with MPNs. **a** The bioprinted butterfly (food dye), leaf (food dye), snowflake (food dye), and eagle with MPNs. **b** The bioprinted nose and vertical sections showing the MPNs. **c** The bioprinted bone and cross/vertical sections showing the MPNs

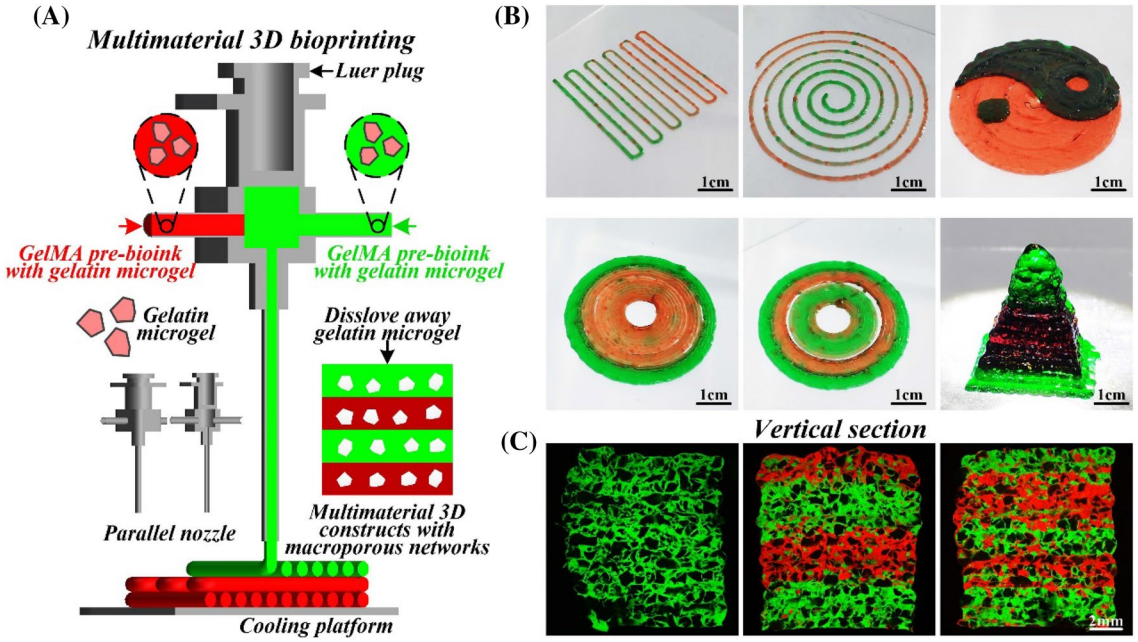

Fig. 5 3D bioprinting multicomponent constructs with MPNs. **a** Schematic of the 3D bioprinting multicomponent constructs with MPNs. **b** The bioprinted multicomponent (food dyes) structures with MPNs. **c** The bioprinted 3D multicomponent constructs with MPNs and vertical sections showing different components and MPNs

manner. Meanwhile, the vertical section views confirmed the presence of MPNs within 3D constructs (Fig. 5c). This strategy may open possibilities in the creation of freeform and heterogeneous constructs on demand. The adaptability of our bioprinting system provides a new level of convenience in fabricating complex constructs with MPNs, allowing for selection from multiple materials as necessary without the need of replacing the nozzles. Together, this enables the production of constructs that closely mimic the composition of real tissues and organs.

Bioactivity of bioprinted cell-laden constructs with mesoscale pore networks

To verify the effectiveness of MPNs for enhancing cell activity, we bioprinted the cell-laden constructs (10 mm × 10 mm × 10 mm) with MPNs and measured cell viability in different sections of the constructs, as displayed schematically in Fig. 6a. We introduced osteoblast (MC3T3-E1, 1.0×10^6 cells/ml) and human umbilical cord vein endothelial cells (HUVECs, 1.0×10^6 cells/ml) into the GelMA pre-bioink and bioprinted cell-laden constructs with MPNs for culture in vitro. To assess cell viability, live/dead staining was performed on day 1, as shown in Fig. 6b, Figures S4, S5 (Supporting Information). These live/dead fluorescence micrographs revealed that the cells were homogeneously distributed within the bioprinted constructs, and MPN structures were preserved. Overall, the cell viability in different sections (left, middle, right) was high. Meanwhile, we found that all sections had viability of at least 85% and that there was no difference across sections through ImageJ software, as shown in Fig. 6c. Furthermore, to study the enhancement of oxygen/nutrient diffusion for cell survival in the constructs with MPNs, HUVEC-laden constructs (1.0×10^6 cells/ml, 3 mm × 3 mm × 3 mm) with/without MPNs were bioprinted and made from molds, respectively. The HUVEC viability encapsulated in constructs with/without MPNS was studied within a period of culture (days 1, 4, and 7), as shown in Fig. 6d, Figure S6 (Supporting Information). And the HUVEC viability was quantified through ImageJ software, as shown in Figure S7 (Supporting Information). In comparison, HUVECs exhibited higher viability within constructs with MPNs as compared with constructs without MPNs, and the difference is more and more obvious with increasing the culture time. Moreover, the HUVEC viability encapsulated in constructs with different void volumes was studied after 4 days of culture. HUVECs survived better within constructs with larger void volume, as shown in Figure S8 (Supporting Information). Additionally, F-actin/DAPI staining was performed to monitor the spreading of the encapsulated cells in the constructs, as shown in Fig. 6e, f, Figures S9, S10 (Supporting Information). As expected, the encapsulated cells in the constructs with MPNs gradually spread to long stripe shapes after 7 days of culture.

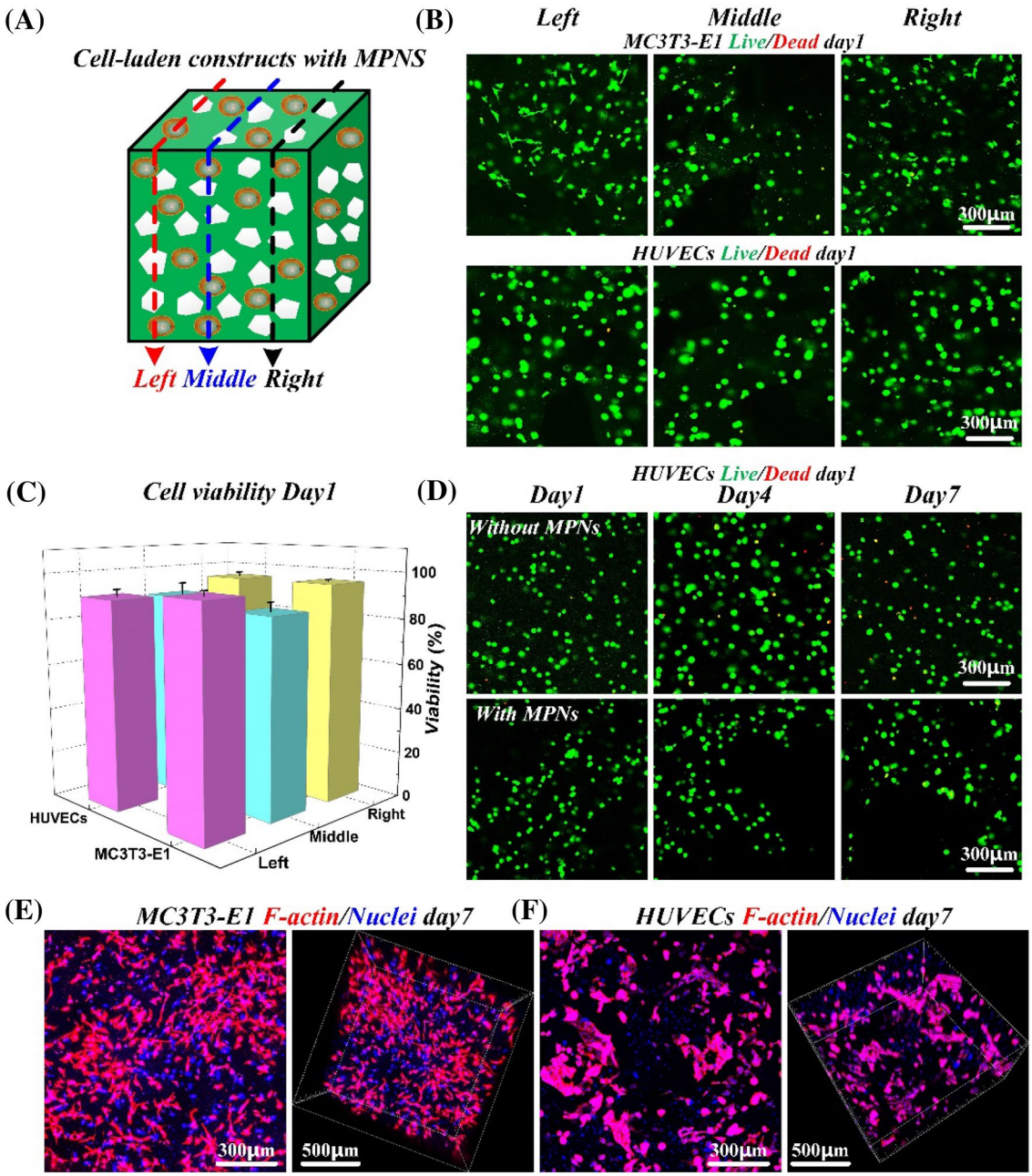

Fig. 6 Bioactivity of cells encapsulated in large-scale constructs. **a** The schematic illustration of left/middle/right sections of the bioprinted cell-laden constructs. **b** After 1 day of culture, live/dead staining of MC3T3-E1 and HUVECs encapsulated in different sections. **c** After 1 day of culture, cell viability of MC3T3-E1 and HUVECs encapsulated in different sections (mean values are presented and the error bars show the SD of independent replicates). **d** Live/dead staining of HUVECs encapsulated in bioprinted constructs with/without MPNs within a period of culture (days 1, 4, and 7). **e** CLSM images showing the spreading of MC3T3-E1 cells. **f** CLSM images showing the spreading of HUVECs

Meanwhile, by comparison, the HUVEC in constructs with MPNs spreads longer than that in constructs without MPNs, as shown in Figure S11 (Supporting Information). These results highlight the ability of MPNs to transport the nutrients/oxygen required for enhancing cell growth. However, when the structure is long-term cultured in vitro or is too large, the ability of the porous structure to diffuse and transfer nutrients/oxygen is limited, which inevitably leads to the death of cells in the center of the structure due to nutrient deficiencies and hypoxia.

Conclusions

In conclusion, we designed a tunable sacrificial gelatin microgel-laden bioink for direct deposition of MPN-containing tissue constructs. Moreover, the all-in-one nozzles allowed for simple bioprinting of multicomponent or multicellular tissue constructs that enabled the formation of complex heterogeneous structures. Furthermore, our 3D bioprinting strategy promoted cell survival in the MPN-containing bioprinted constructs, as well as corresponding in vivo-like behavior of the encapsulated cells. Prospectively, porous structures may have a good repair effect in vivo and it needs to be verified by animal experiments in the future work. In view of these findings, we believe that our 3D bioprinting strategy based on sacrificial gelatin microgel-laden bioink could have wide applications in engineering various tissue constructs for diverse applications in tissue engineering.

Acknowledgements This work was sponsored by the National Nature Science Foundation of China (Nos. U1609207, 81827804).

Compliance with ethical standards

Conflict of interest The authors declare that they have no conflict of interest.

Ethical approval This study does not contain any studies with human or animal subjects performed by any of the authors.

References

1. Kang H, Lee S, Ko I, Kengla C, Yoo J, Atala A (2016) A 3D bioprinting system to produce human-scale tissue constructs with structural integrity. Nat Biotechnol 34:312–319
2. Murphy S, Atala A (2014) 3D bioprinting of tissues and organs. Nat Biotechnol 32:773–785
3. Derby B (2012) Printing and prototyping of tissues and scaffolds. Science 338:921–926
4. Lee A, Hudson AR, Shiwarski DJ, Tashman JW, Hinton TJ, Yerneni S, Bliley JM, Campbell PG, Feinberg AW (2019) 3D bioprinting of collagen to rebuild components of the human heart. Science 365:482–487
5. Kolesky DB, Homan KA, Skylar-Scott MA, Lewis JA (2016) Three-dimensional bioprinting of thick vascularized tissues. Proc Natl Acad Sci USA 113:3179–3184
6. Mandrycky C, Wang Z, Kim K, Kim D (2016) 3D bioprinting for engineering complex tissues. Biotechnol Adv 34:422–434
7. Pati F, Jang J, Ha D, Kim S, Rhie J, Shim J, Kim D, Cho D (2014) Printing three-dimensional tissue analogues with decellularized extracellular matrix bioink. Nat Commun 5:3935
8. He Y, Xie M, Gao Q, Fu J (2019) Why choose 3D bioprinting? Part I: a brief introduction of 3D bioprinting for the beginners. Biodes Manuf 2:221–224
9. Gao Q, Zhao P, Zhou R, Wang P, Fu J, He Y (2019) Rapid assembling organ prototypes with controllable cell-laden multiscale sheets. Biodes Manuf 2:1–9
10. Hospodiuk M, Dey M, Sosnoski D, Ozbolat IT (2017) The bioink: a comprehensive review on bioprintable materials. Biotechnol Adv 35:217–239
11. Gungor-Ozkerim P, Inci I, Zhang Y, Khademhosseini A, Dokmeci M (2018) Bioinks for 3D bioprinting: an overview. Biomater Sci 6:915–946
12. Hölzl K, Lin S, Tytgat L, Vlierberghe S, Gu L, Ovsianikov A (2016) Bioink properties before, during and after 3D bioprinting. Biofabrication 8:032002
13. Ferris FJ, Gilmore KJ, Beirne S, McCallum D, Wallace GG, Panhuis M (2013) Bio-ink for on-demand printing of living cells. Biomater Sci 1:224–230
14. Chung JHY, Naficy S, Yue Z, Kapsa R, Quigley A, Moulton SE, Wallace GG (2013) Bio-ink properties and printability for extrusion printing living cells. Biomater Sci 1:763–773
15. Fedorovich NE, Schuurman W, Wijnberg HM, Prins H-J, van Weeren PR, Malda J, Alblas J, Dhert WJA (2012) Biofabrication of osteochondral tissue equivalents by printing topologically defined, cell-laden hydrogel scaffolds. Tissue Eng Part C 18:33–44
16. Eiselt P, Yeh J, Latvala RK, Shea LD, Mooney DJ (2000) Porous carriers for biomedical applications based on alginate hydrogels. Biomaterials 21:1921–1927
17. He Y, Yang F, Zhao H, Gao Q, Xia B, Fu J (2016) Research on the printability of hydrogels in 3D bioprinting. Sci Rep 6:29977
18. Douglas AM, Fragkopoulos AA, Gaines MK, Lyon LA, Fernandez-Nieves A, Barker TH (2017) Dynamic assembly of ultrasoft colloidal networks enables cell invasion within restrictive fibrillar polymers. Proc Natl Acad Sci USA 114:885–890
19. Xin S, Wyman OM, Alge DL (2018) Assembly of PEG microgels into porous cell-instructive 3D scaffolds via thiol-ene click chemistry. Adv Healthc Mater 7:1800160
20. Zeltinger J, Sherwood JK, Graham DA, Müeller R, Griffith LG (2001) Effect of pore size and void fraction on cellular adhesion, proliferation, and matrix deposition. Tissue Eng 7:557–572
21. Al-Munajjed AA, Hien M, Kujat R, Gleeson JP, Hammer J (2008) Influence of pore size on tensile strength, permeability and porosity of hyaluronan-collagen scaffolds. J Mater Sci Mater Med 19:2859–2864
22. Huebsch N, Lippens E, Lee K, Mehta M, Koshy ST, Darnell MC, Desai RM, Madl CM, Xu M, Zhao X, Chaudhuri O, Verbeke C, Kim W, Alim K, Mammoto A, Ingber DE, Duda GN, Mooney DJ (2015) Matrix elasticity of void-forming hydrogels controls transplanted-stem-cell-mediated bone formation. Nat Mater 14:1269–1277
23. Ying G, Jiang N, Maharjan S, Yin Y, Chai R, Cao X, Yang J, Miri AK, Hassan S, Zhang Y (2018) Aqueous two-phase emulsion bioink-enabled 3D bioprinting of porous hydrogels. Adv Mater 30:1805460
24. Cooperstein I, Layani M, Magdassi S (2015) 3D printing of porous structures by UV-curable O/W emulsion for fabrication of conductive objects. J Mater Chem C 3:2040–2044
25. Sears NA, Dhavalikar PS, Cosgriff-Hernandez EM (2016) Emulsion inks for 3D printing of high porosity materials. Macromol Rapid Commun 37:1369–1374
26. Armstrong JP, Burke M, Carter BM, Davis SA, Perriman AW (2016) 3D bioprinting using a templated porous bioink. Adv Healthc Mater 5:1724–1730
27. King WJ, Toepke MW, Murphy WL (2011) Facile formation of dynamic hydrogel microspheres for triggered growth factor delivery. Acta Biomater 7:975–985
28. Chen YC, Lin RZ, Qi H, Yang Y, Bae H, Melero-Martin JM, Khademhosseini A (2012) Functional human vascular network generated in photocrosslinkable gelatin methacrylate hydrogels. Adv Funct Mater 22:2027–2039

29. Klotz BJ, Gawlitta D, Rosenberg AJ, Malda J, Melchels FP (2016) Gelatin-methacryloyl hydrogels: towards biofabrication-based tissue repair. Trends Biotechnol 34:394–407
30. Kim SH, Yeon YK, Lee JM, Chao JR, Lee YJ, Seo YB, Sultan MT, Lee OJ, Lee JS, Yoon S, Hong I, Khang G, Lee SJ, Yoo JJ, Park CH (2018) Precisely printable and biocompatible silk fibroin bioink for digital light processing 3D printing. Nat Commun 9:1620
31. Yue K, Santiago GT, Alvarez MM, Tamayol A, Annabi N, Khademhosseini A (2015) Synthesis, properties, and biomedical applications of gelatin methacryloyl (GelMA) hydrogels. Biomaterials 73:254–271
32. Noshadi I, Hong S, Sullivan KE, Sani ES, Portillo-Lara R, Tamayol A, Shin SR, Gao AE, Stoppel WL, Black LD III (2017) In vitro and in vivo analysis of visible light crosslinkable gelatin methacryloyl (GelMA) hydrogels. Biomater Sci 5:2093–2105
33. Zhu W, Qu X, Zhu J, Ma X, Patel S, Liu J, Wang P, Lai CSE, Gou M, Xu Y, Zhang K, Chen S (2017) Direct 3D bioprinting of prevascularized tissue constructs with complex microarchitecture. Biomaterials 124:106–115
34. Lim KS, Levato R, Costa PF, Castilho MD, Alcala-Orozco CR, Dorenmalen KMA, Melchels FPW, Gawlitta D, Hooper GJ, Malda J, Woodfield TBF (2018) Bio-resin for high resolution lithography-based biofabrication of complex cell-laden constructs. Biofabrication 10:034101
35. Ouyang L, Highley CB, Sun W, Burdick JA (2017) A generalizable strategy for the 3D bioprinting of hydrogels from nonviscous photo-crosslinkable inks. Adv Mater 29:1604983
36. Yin J, Yan M, Wang Y, Fu J, Suo H (2018) 3D bioprinting of low-concentration cell-laden gelatin methacrylate (GelMA) bioinks with a two-step cross-linking strategy. ACS Appl Mater Interfaces 10:6849–6857
37. Shao L, Gao Q, Zhao H, Xie C, Fu J, Liu Z, Xiang M, He Y (2018) Fiber-based mini tissue with morphology-controllable GelMA microfibers. Small 14:1802187
38. Shao L, Gao Q, Xie C, Fu J, Xiang M, He Y (2019) Bioprinting of cell-laden microfiber: can it become a standard product? Adv Healthc Mater 8:1900014
39. Lee BH, Lum N, Seow LY, Lim PQ, Tan LP (2016) Synthesis and characterization of types A and B gelatin methacryloyl for bioink applications. Materials 9:797
40. Meyers MA, Chen P, Lin AY, Seki Y (2008) Biological materials: structure and mechanical properties. Prog Mater Sci 53:1–206